Applied Physics Letters ARTICLE pubs.aip.org/aip/apl

THz cyclotron resonance of a 2D hole gas in a GaN/AlN heterostructure

Cite as: Appl. Phys. Lett. **126**, 213102 (2025); doi: 10.1063/5.0273413
Submitted: 31 March 2025 · Accepted: 6 May 2025 ·
Published Online: 28 May 2025

View Online Export Citation CrossMark

J. Wang,[1] D. G. Rickel,[1] C. F. C. Chang,[2] Z. Zhang,[3] P. Peng,[4] Y. Huang,[4] A. K. Azad,[4] D. Jena,[3,5,6,a)] H. G. Xing,[3,5,6,a)] and S. A. Crooker[1,a)]

AFFILIATIONS

[1]National High Magnetic Field Laboratory, Los Alamos National Lab, Los Alamos, New Mexico 87545, USA
[2]Department of Physics, Cornell University, Ithaca, New York 14853, USA
[3]School of Electrical and Computer Engineering, Cornell University, Ithaca, New York 14853, USA
[4]Center for Integrated Nanotechnologies, Los Alamos National Lab, Los Alamos, New Mexico 87545, USA
[5]Department of Materials Science and Engineering, Cornell University, Ithaca, New York 14853, USA
[6]Kavli Institute at Cornell for Nanoscale Science, Ithaca, New York 14853, USA

[a)]**Authors to whom correspondence should be addressed:** djena@cornell.edu; grace.xing@cornell.edu; and crooker@lanl.gov

ABSTRACT

The recent discovery of highly conducting two-dimensional hole gases (2DHGs) in GaN/AlN heterojunctions has opened the door to efficient complementary GaN electronics, a long-standing challenge in wide-bandgap semiconductor device physics. Electrical transport studies and simulations indicate that both heavy- and light-hole valence bands are occupied in these 2DHGs, but direct experimental characterization of the fundamental parameters of the mobile holes remains at an early stage. Here, we use time-domain terahertz spectroscopy and pulsed magnetic fields up to 31 T to directly measure cyclotron resonance of the mobile 2D holes in these GaN-based 2DHGs at low temperature (8 K), revealing key material properties including effective masses, densities, scattering times, and mobilities.

Gallium nitride (GaN) has emerged as one of the most impactful semiconductors in modern materials science, due to its wide bandgap, exceptional thermal stability, and high electron mobility. These properties have made GaN as a cornerstone material in a broad range of applications, ranging from light-emitting devices to high speed transistors to power electronics.[1–3] Spontaneous polarization effects at GaN-based heterointerfaces can create high-mobility two-dimensional electron gases (2DEGs),[4,5] enabling, for example, field-effect transistors operating at microwave frequencies.[6] However, the advance of GaN-based electronics has been limited by the challenge of realizing the analogous hole-doped (*p*-type) counterpart of such heterostructures, which is crucial to achieving integrated complementary electronics. The difficulty arises from GaN's wide bandgap, which results in valence bands with large masses lying deep in energy, making them difficult to chemically dope and inherently low in mobility.[7]

Recently, however, high-density 2D hole gases (2DHG) were realized in epitaxially grown GaN/AlN heterostructures without any doping.[8] The 2DHG carrier density is one of the largest among all known semiconductors, leading to high sheet conductance despite low carrier mobilities. While theoretical modeling suggests the splittings and dispersions of the valence bands in GaN/AlN structures, experimental measurements of the 2DHG properties are still at an early stage. In particular, one of the most fundamental material parameters relevant to any 2D system of mobile carriers is their effective mass m_{eff}, which in GaN-based 2DHGs is typically assumed from theoretical modeling,[9] and was only very recently inferred from Shubnikov–de Haas (SdH) oscillations in electrical resistance.[10]

Arguably the most direct experimental measure of m_{eff} arises from studies of cyclotron resonance (CR),[11] where the frequency of cyclotron motion of the mobile carriers, ω_c, in an applied magnetic field B directly reveals their mass via $\omega_c = eB/m_{\text{eff}}$. Widely employed for decades in narrower-gap semiconductors using small B and microwave (GHz) frequencies,[12] CR is a contactless measurement amenable for rapid feedback on the quality and uniformity of epitaxially grown wafers. However, resolving the CR of holes in GaN is challenging because it requires both large (THz) frequencies and very large B (many tens of teslas). This is because holes in GaN have short scattering times (~ 1 ps), such that the linewidth of their CR peak in the frequency domain is

quite broad (∼1 THz), and also because holes in GaN are expected to have large masses, so that large B is required to shift the CR peak by an appreciable fraction of its linewidth so that the cyclotron shift can be resolved. Moreover, the 2DHGs in GaN populate *both* heavy-hole (*hh*) and light-hole (*lh*) valence bands, meaning once again that large B are needed to spectrally distinguish the CR peaks from the two hole species. These challenges stand in contrast to CR studies of high-mobility lighter-mass 2D holes in GaAs[13] or Ge,[14] for which low fields suffice.

Finally, we emphasize that the properties of mobile *hh* and *lh* carriers, such as their precise masses, densities, and scattering times, depend sensitively on the band splitting and 2DHG Fermi energy, and therefore on the details of the heterostructure layers and growth parameters. Thus, it is desirable to measure these key parameters in a direct way, and CR in high B provides such a route. To this end, we perform time-domain THz spectroscopy of a GaN/AlN 2DHG in pulsed magnetic fields up to 31 T and resolve the CR of both heavy and light holes. These data reveal the effective masses, densities, scattering times, and mobilities of the mobile holes. Our results complement and are compared to values recently inferred from electrical transport studies of related 2DHGs.[10,15]

Figure 1(a) depicts the GaN/AlN 2DHG structure grown by molecular-beam epitaxy on an AlN substrate.[8] It comprises an AlN buffer layer (700 nm thick), followed by an undoped 8.2 nm GaN layer. A high density 2D sheet of mobile holes is created by the large intrinsic and strain-induced polarization at the GaN/AlN interface.[4,5,16] Figure 1(b) shows the calculated splitting and dispersion of the GaN valence bands near the interface,[17] indicating that the 2DHG populates both *hh* and *lh* valence bands.

The experimental setup is shown in Fig. 1(c). The samples are mounted in vacuum on the sapphire cold finger of a small helium cryostat, which is positioned within the 15 mm bore of a small pulsed electromagnet. The magnet consists of 144 turns of high-strength copper–silver wire (1 mm diameter), and is powered by a purpose-built 4.4 mF capacitor bank.[18,19] The commercial (Toptica) THz system is based on electronically controlled optical sampling (ECOPS), which permits detection of an entire THz pulse waveform, $E(t)$, in tens-of-microseconds timescales, and at repetition rates up to 1.6 kHz.[20,21] Picosecond pulses of free-space THz radiation are generated in a fiber-coupled photoconducting antenna, then linearly polarized (vertically, at 0°) and focused through the sample. The transmitted THz pulses then pass through a second linear polarizer (oriented at ±45°), and their final electric field waveform $E(t)$ is detected by a photoconducting receiver. Measurements are performed in the Faraday geometry, i.e., with B applied along the direction of light propagation and perpendicular to the sample surface.

Figure 1(d) shows a typical field profile of a 31 T magnet pulse, along with the THz signal. An expanded view of a measured THz waveform $E(t)$ at peak field is shown in Fig. 1(e). The usable bandwidth of the THz pulses spans approximately 0.4–1.6 THz. To improve signal-to-noise, the THz waveforms are typically averaged over 10–20 magnet pulses.

It is essential in these studies to measure the sample's optical conductivity, $\sigma(\omega)$, in a basis of circular optical polarization, as it is the natural eigenbasis of cyclotron motion. We therefore measure the complex (real and imaginary) THz transmission spectrum, $T(\omega)$, in a ±45° linearly polarized basis (by rotating P2), and then transform into a left- and right-circular basis. First, the normalized THz transmission is obtained as $T(\omega,B)/T(\omega,0) = \mathcal{F}[E(t,B)]/\mathcal{F}[E(t,0)]$, where $\mathcal{F}[E(t,B)]$ and $\mathcal{F}[E(t,0)]$ are the (complex-valued) Fourier transforms of the THz waveforms measured in applied field B and in $B = 0$,

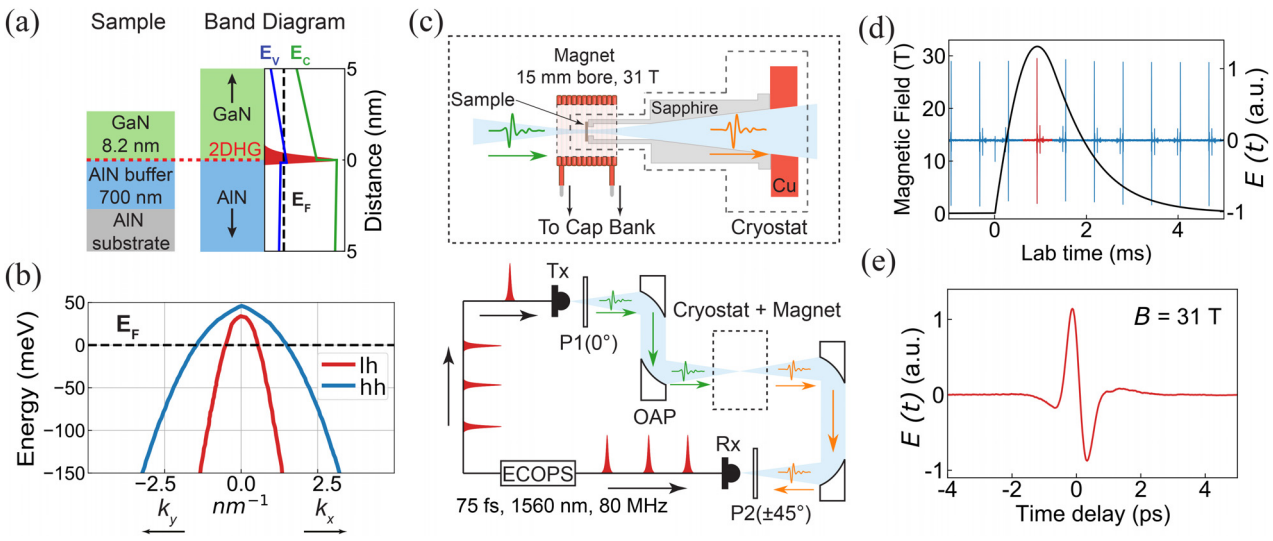

FIG. 1. (a) Schematic of the sample structure and band alignment. The 2DHG is created by the large intrinsic and strain-induced polarization at the GaN/AlN interface. (b) Schematic of the calculated dispersion of the GaN valence bands; the 2DHG populates both heavy- and light-hole bands. (c) Experimental schematic. Samples are mounted on the sapphire cold finger of a helium cryostat, the end of which is positioned within a small pulsed magnet. An ECOPS-based time-domain THz spectrometer generates THz optical pulses using a fiber-coupled photoconducting transmitter (Tx). The THz light is collimated and focused through the sample by off-axis parabolic (OAP) mirrors, and then re-focused to a THz receiver (Rx). Wire-grid linear polarizers P1 and P2 control the THz polarization (set to 0° and ±45°, respectively). (d) The field profile of a 31 T magnet pulse, and the simultaneously measured THz electric field $E(t)$, shown vs lab time. (e) Expanded view of the measured THz electric field $E(t)$ measured at 31 T, plotted vs optical time delay.

respectively. This is performed with P2 oriented at $+45°$ and then at $-45°$. Then, the diagonal and off diagonal components of the sample's linear transmission matrix are calculated via $T_{\pm 45°} = (T_{xx} \pm T_{xy})/\sqrt{2}$. Right- and left-circular transmission spectra are then obtained using $T_{r,l}(\omega) = T_{xx}(\omega) \pm i T_{xy}(\omega)$, from which the right- and left-circular optical conductivity, $\sigma_r(\omega)$ and $\sigma_l(\omega)$, are determined (described in more detail below).

Cyclotron resonance is most clearly represented when $\sigma_r(\omega)$ and $\sigma_l(\omega)$ are plotted together vs positive and negative frequencies, respectively.[19,22,23] In the simplest model of CR, each mobile carrier species contributes a Drude-like conductivity peak centered at $\omega = 0$ at $B = 0$. This Drude peak shifts to higher frequency with increasing B at a rate that is inversely proportional to its effective mass m_{eff}, a consequence of the 2D electronic density of states breaking up into equally spaced Landau levels that are separated by the cyclotron frequency. At high B, CR from carriers with different masses can therefore be spectrally distinguished and accurately analyzed.

Figure 2(a) shows a simple simulation for a minimal model system containing both heavy and light holes. For *each* carrier species, the Drude model gives a complex conductivity,

$$\sigma(\omega, B) = \frac{\epsilon_0 \omega_p^2}{1/\tau - i(\omega - \omega_c)}, \tag{1}$$

which is a Lorentzian oscillator centered at the cyclotron frequency $\omega_c = eB/m_{\text{eff}}$, where e is the electron charge (positive for holes). The width of the Drude peak in the real part of $\sigma(\omega)$ is given by the inverse carrier scattering time $1/\tau$, and the spectral weight of each carrier species is given by its plasma frequency $\omega_p^2 = Ne^2/\epsilon_0 m_{\text{eff}}$, where N is the carrier density. The cyclotron energy $\hbar\omega_c$ is just the spacing between the Landau levels that develop when $B > 0$. When multiple carrier species exist, each species contributes to $\sigma(\omega)$ independently.

Figure 2(a) shows $\sigma(\omega)$ for a model system containing both heavy and light holes, using $m_{lh} = 0.5\, m_e$ and $m_{hh} = 2.5\, m_e$ (values estimated from band structure calculations of GaN). For simplicity, both carrier species are assigned the same spectral weight and equal scattering times $\tau = 0.4$ ps (estimated from Hall mobility studies). At $B = 0$, the Drude conductivity peaks of both species are centered at zero frequency ($\omega_c = 0$), forming a single peak. However, when $B > 0$, the two Drude peaks shift in frequency and separate due to their different masses. In this example, the two conductivity peaks become well separated and spectrally resolvable in high fields $B \gtrsim 20$ T, enabling the characterization of both carrier masses, as well as their spectral weights and scattering times.

The experimentally measured optical conductivity from the 2DHG structure is shown in Fig. 2(b). Both Re[σ] and Im[σ] at high magnetic fields closely follow the trends anticipated by the minimal model described earlier [cf. Fig. 2(a)]. The data clearly show the emergence and separation of two distinct conductivity peaks shifting toward positive frequencies, confirming the presence of both heavy and light holes in the 2DHG. The dashed lines show fits to the data based on the minimal Drude model discussed earlier.

The fitted CR frequencies, shown in Fig. 3, increase linearly with B, with slope that reveals m_{eff}. We find that $m_{hh} = 2.6m_e$ and $m_{lh} = 0.57m_e$. We emphasize that these data represent the first measurement of hole CR in GaN-based semiconductors, which is made experimentally challenging by the larger masses and lower mobilities of holes (compared, e.g., to mobile electrons in GaN, or to carriers in narrower-gap semiconductors), and the consequent need for both high B and broad (THz) detection bandwidths to spectrally distinguish their broad Drude conductivity peaks.

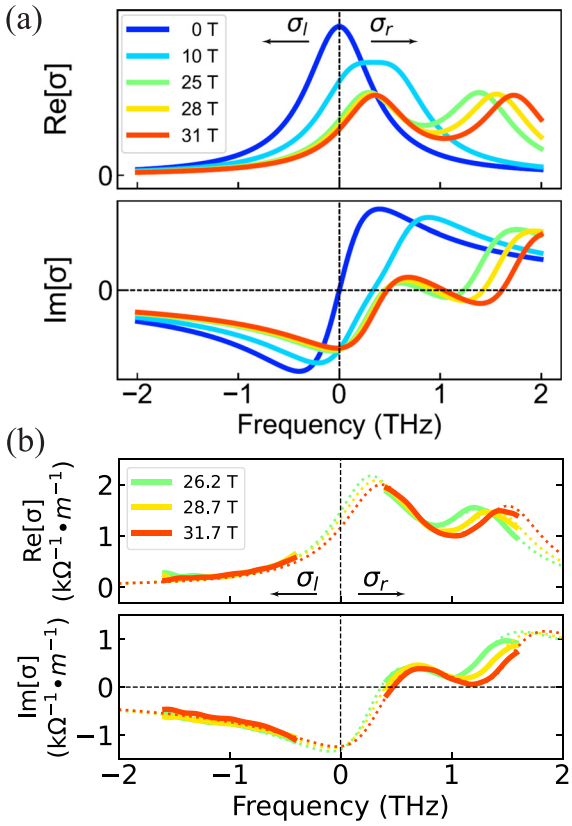

FIG. 2. (a) Simulation of the left- and right-circularly polarized complex optical conductivity, $\sigma_{l,r}(\omega)$, from a 2D layer containing two species of mobile hole carriers having effective masses $m_{\text{eff}} = 0.5m_e$ and $2.5m_e$. Each species is assigned the same spectral weight, and same scattering time $\tau = 0.4$ ps. Negative and positive frequencies correspond to $\sigma_l(\omega)$ and $\sigma_r(\omega)$, respectively. Each species contributes a Drude-like conductivity (with real part Re[σ] and imaginary part Im[σ]), given by a complex Lorentzian oscillator centered at the cyclotron frequency $\omega_c = eB/m_{\text{eff}}$. The conductivity peaks from the two species become separated and easier to individually resolve at high B, due to their different m_{eff} and ω_c. (b) The measured complex optical conductivity of the 2DHG, at 8 K and in the high B indicated. The dashed lines are fits using a simple Drude model with both *hh* and *lh* carriers.

In addition to effective mass, the spectrally resolved CR peaks in $\sigma(\omega)$ also reveal the heavy- and light-hole densities N, and their scattering times τ from which mobilities μ can be independently determined, complementing and validating material parameters inferred from electrical transport studies. These important parameters are measured as follows: As outlined above, the complex optical transmission spectrum in applied B, normalized to its value at $B = 0$, is obtained as $T(\omega, B)/T(\omega, 0) = \mathcal{F}[E(t, B)]/\mathcal{F}[E(t, 0)]$. For 2D mobile carriers at the interface between two media, this quantity can be approximated as[24]

$$\frac{T(\omega, B)}{T(\omega, 0)} = \frac{\sigma(\omega, 0) + Y}{\sigma(\omega, B) + Y}, \tag{2}$$

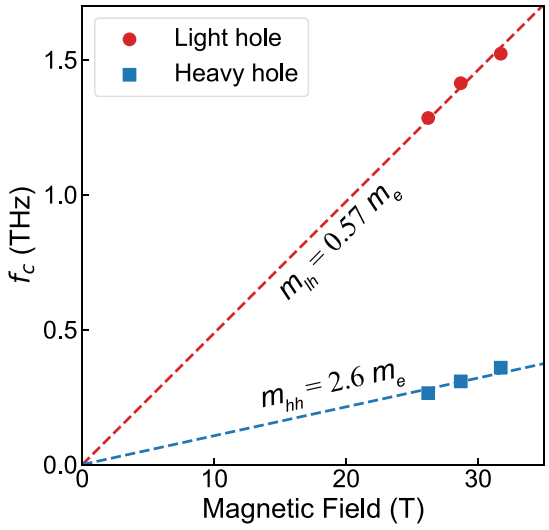

FIG. 3. The measured cyclotron frequencies of light and heavy holes in the 2DHG. The dashed lines are linear fits to $f_c = \omega_c/2\pi = eB/2\pi m_{\text{eff}}$, from which the heavy- and light-hole effective masses are directly revealed.

where σ is the sheet conductivity, and $Y = Y_1 + Y_2$ is the effective admittance defined as the sum of the admittances of the two media. Here, the 2DHG can be taken to reside at an interface between vacuum ($Y_1 = Y_{\text{vac}} = 1/377\Omega$) and the AlN substrate ($Y_2 = n_{\text{AlN}} Y_{\text{vac}} \approx 2.8 Y_{\text{vac}}$), because the ultra-thin semiconducting GaN layer gives little contribution at 8 K. The sheet conductivity is given by a two-carrier Drude model,

$$\sigma(\omega, B) = \frac{\epsilon_0 \omega_{p,hh}^2}{1/\tau_{hh} - i(\omega - \omega_{c,hh})} + \frac{\epsilon_0 \omega_{p,lh}^2}{1/\tau_{lh} - i(\omega - \omega_{c,lh})}. \quad (3)$$

These two expressions give the normalized complex transmission spectrum as a function of m_{hh}, m_{lh}, N_{hh}, N_{lh}, τ_{hh}, and τ_{lh}. All six parameters can be extracted by simultaneously fitting the real and imaginary parts of the measured complex transmission at high B, and $\sigma(\omega)$ can be reconstructed by substituting the fit parameters into Eq. (3).

The ability to extract all six parameters from a single fit is aided by two noteworthy advantages of the THz experiment: First, large B forces the spectral separation of the *hh* and *lh* CR peaks, which can then be fit essentially independently. For 2DHGs in GaN, fields of order 30 T are needed because both carriers have relatively large mass and short scattering times that lead to broad CR peaks. By forcing the spectral separation of the CR peaks, not only m_{eff} but also τ and N (via the spectral weight) can be more accurately determined for each hole species. We emphasize that without independent knowledge of m_{eff} that is provided by the cyclotron shift, the spectral weight reveals only the ratio N/m_{eff}.

Second, we measure the *complex-valued* THz transmission in a circular polarization basis. Simultaneously fitting both the real and imaginary transmission spectrum naturally puts additional constraints on the fit and improves its accuracy. This is possible in time-domain THz studies because both amplitude *and* phase are encoded in the measured electric field $E(t)$, in contrast to phase-insensitive methods that detect only optical intensities ($\propto EE^*$).

Table I shows the material parameters of these 2D holes, as determined by our CR experiments. Mobilities are calculated from the measured scattering times via $\mu = e\tau/m_{\text{eff}}$. We note that the larger uncertainty in the parameters m_{hh} and N_{hh} is due to the fact that the peak of the heavy-hole CR does not quite fall within the detection range [see Fig. 2(b)], which makes it more difficult to independently fit the peak's amplitude and central frequency. To improve accuracy, we measured the low-temperature THz optical conductivity of the GaN/AlN 2DHG structure at $B = 0$, referenced to a bare AlN substrate, and extracted the *total* spectral weight from both carrier species by fitting to a single Drude peak. This is a reasonable approach for a two-carrier system when both species have similar scattering rates. The total spectral weight is then used as an additional constraint, which reduces uncertainty in N_{hh} and improves the fitting of m_{hh}.

For comparison, Table I also shows the corresponding heavy- and light-hole parameters reported very recently in two electrical transport studies of similar GaN/AlN 2DHGs grown in the same MBE chamber[10,15] (note, however, that the layer thicknesses were not exactly the same, and some structures used in these transport studies also incorporated an additional Mg-doped *p*-type GaN capping layer to improve electrical contact to the 2DHG). In Ref. 15, magneto-transport measurements up to 9 T were fit to a two-carrier model of the Hall effect, from which Hall mobilities and carrier densities were inferred. In Ref. 10, Shubnikov–de Haas (SdH) quantum oscillations from both heavy and light 2D holes were measured in pulsed magnetic fields to 72 T, providing a measure of carrier densities (via the SdH oscillation frequency) and masses (via the temperature-dependence of the SdH amplitude), along with an estimate of the quantum scattering time τ_q (via the field-dependence of the SdH oscillations). Note that τ_q is generally smaller than transport scattering times τ_t, determined by, e.g., Hall effects, because quantum oscillations are sensitive to *all* scattering mechanisms and sample inhomogeneities.[25–28]

Overall, Table I shows a general agreement between the parameters inferred from these different measurement techniques on these different 2DHG samples. Light hole masses and carrier densities are in reasonable agreement. Low-temperature transport mobilities are in the same general range ($\approx 300\ \text{cm}^2/\text{V}\cdot\text{s}$ for heavy holes, and on the order of $1500\ \text{cm}^2/\text{V}\ \text{s}$ for light holes), with variations likely arising from differences in sample quality. As expected, the quantum scattering times

TABLE I. Heavy-hole and light-hole parameters determined by cyclotron resonance on this GaN/AlN 2DHG. Also listed are parameters inferred from electrical transport studies of similar but different GaN/AlN 2DHGs. All reported mobilities are low-temperature values ($T < 10$ K).

	This work	Reference 10	Reference 15
$m_{hh}(m_e)$	2.6±0.2	1.92 ± 0.16	N/A
$m_{lh}(m_e)$	0.57±0.01	0.53 ± 0.01	N/A
N_{hh} (10^{13}cm^{-2})	4.6±0.2	3.8 ± 0.1	∼4
N_{lh} (10^{13}cm^{-2})	0.65±0.03	0.8 ± 0.01	∼0.5
τ_{hh} (10^{-13}s)	3.9±0.2 (τ_t)	1.7–2.4 (τ_q)	N/A
τ_{lh} (10^{-13}s)	4.0±0.2 (τ_t)	1.5 (τ_q)	N/A
μ_{hh} ($\text{cm}^2/\text{V}\cdot\text{s}$)	262 ±30 (μ_t)	∼400 (μ_t) 167–200 (μ_q)	∼300 (μ_t)
μ_{lh} ($\text{cm}^2/\text{V}\cdot\text{s}$)	1242 ±80 (μ_t)	∼1900 (μ_t) 368 ± 14 (μ_q)	∼1400 (μ_t)

inferred from SdH studies are shorter than scattering times determined by transport or CR. Where the CR and SdH experiments differ most noticeably is in the determination of the heavy-hole mass m_{hh} (2.6 m_e vs 1.92 m_e, respectively). In general, masses measured by SdH oscillations reflect the quasiparticle dispersion renormalized by both electron–phonon and electron–electron interactions, and are therefore often found to be heavier than the bare band mass.[29] However, Kohn's theorem states that in a Galilean-invariant system, the cyclotron frequency ω_c is unaffected by electron–electron interactions.[30] Although electron–electron interactions *can* enhance the cyclotron mass in high-density systems where Galilean invariance no longer holds,[31] or in systems that have non-parabolic bands[32] (in GaN, the bands are not perfectly parabolic), it is still somewhat unexpected to infer a smaller mass from SdH quantum oscillations in comparison with a cyclotron resonance measurement. Despite the increased uncertainty in our determination of m_{hh} by CR (discussed above), a 30% discrepancy seems to be in excess of experimental error and may hint at interesting underlying physics. Further investigations of CR in higher magnetic fields, where the heavy-hole CR peak can be more completely resolved, are needed to resolve this puzzle.

In summary, we directly measured the cyclotron resonance of a 2D hole gas in a GaN/AlN heterojunction by THz spectroscopy in pulsed magnetic fields up to 31 T and revealed the effective masses, densities, scattering times, and mobilities of both heavy and light 2D holes. These are important material parameters for the design and engineering of future complementary GaN-based electronics and photonics. Our results are in broad agreement with parameters inferred from recent electrical transport studies, with the exception of an intriguing difference in m_{hh} that invites further exploration of this system. This experimental capability demonstrates a viable method to characterize wide-bandgap semiconductors, such as *p*-type ZnO and Ga_2O_3, which have heavier carrier masses, and a path to study the electron–electron interactions in correlated systems through the direct evaluation of cyclotron mass.

S.A.C. and J.W. gratefully acknowledge support from the U.S. Department of Energy (DOE) through the Basic Energy Sciences "Science of 100 T" program. The National High Magnetic Field Laboratory is supported by the National Science Foundation (NSF) under Grant No. DMR-2128556, the State of Florida, and the U.S. DOE. We thank Vladimir Protasenko for help with the operation of the molecular beam epitaxy system. Work at Cornell University was supported in part by SUPREME, one of the seven centers in JUMP 2.0, a Semiconductor Research Corporation (SRC) program sponsored by DARPA. We also made use of the Cornell Center for Materials Research Shared Facilities (Grant No. DMR-1719875).

AUTHOR DECLARATIONS

Conflict of Interest

The authors have no conflicts to disclose.

Author Contributions

J. Wang: Investigation (lead); Writing – original draft (equal). **D. G. Rickel:** Investigation (supporting). **C. F. C. Chang:** Investigation (supporting). **Z. Zhang:** Investigation (supporting). **P. Peng:** Investigation (supporting). **Y. Huang:** Investigation (supporting). **A. K. Azad:** Investigation (supporting). **D. Jena:** Conceptualization (equal); Supervision (equal). **H. G. Xing:** Conceptualization (equal); Supervision (equal). **S. A. Crooker:** Conceptualization (equal); Supervision (equal); Writing – review & editing (equal).

DATA AVAILABILITY

The data that support the findings of this study are available from the corresponding authors upon reasonable request.

REFERENCES

[1]E. A. Jones, F. F. Wang, and D. Costinett, "Review of commercial GaN power devices and GaN-based converter design challenges," IEEE J. Emerg. Sel. Top. Power Electron. **4**, 707 (2016).
[2]U. K. Mishra, L. Shen, T. E. Kazior, and Y.-F. Wu, "GaN-based RF power devices and amplifiers," Proc. IEEE **96**, 287 (2008).
[3]G. Fasol, "Room-temperature blue gallium nitride laser diode," Science **272**, 1751 (1996).
[4]O. Ambacher, J. Smart, J. R. Shealy, N. G. Weimann, K. Chu, M. Murphy, W. J. Schaff, and L. F. Eastman, "Two-dimensional electron gases induced by spontaneous and piezoelectric polarization charges in N- and Ga-face AlGaN/GaN heterostructures," J. Appl. Phys. **85**, 3222 (1999).
[5]F. Bernardini, V. Fiorentini, and D. Vanderbilt, "Spontaneous polarization and piezoelectric constants of III-V nitrides," Phys. Rev. B **56**, R10024 (1997).
[6]E. A. Jones, F. Wang, and B. Ozpineci, "Application-based review of GaN HFETs," in *IEEE Workshop on Wide Bandgap Power Devices and Applications* (IEEE, Knoxville, TN, 2014), pp. 24–29.
[7]J. O. Song, J.-S. Ha, and T.-Y. Seong, "Ohmic-contact technology for GaN-based light-emitting diodes: Role of P-type contact," IEEE Trans. Electron Devices **57**, 42 (2010).
[8]R. Chaudhuri, S. J. Bader, Z. Chen, D. A. Muller, H. G. Xing, and D. Jena, "A polarization-induced 2D hole gas in undoped gallium nitride quantum wells," Science **365**, 1454–1457 (2019).
[9]M. Suzuki, T. Uenoyama, and A. Yanase, "First-principles calculations of effective-mass parameters of AlN and GaN," Phys. Rev. B **52**, 8132 (1995).
[10]C. F. C. Chang, J. E. Dill, Z. Zhang, J.-C. Chen, N. Pieczulewski, S. J. Bader, O. A. Valenzuela, S. A. Crooker, F. F. Balakirev, R. D. McDonald, J. Encomendero, D. A. Muller, F. Giustino, D. Jena, and H. G. Xing, "Quantum oscillations of holes in GaN," arXiv:2501.16213 (2025).
[11]D. J. Hilton, T. Arikawa, and J. Kono, "Cyclotron resonance," in *Characterization of Materials*, edited by E. N. Kaufmann (John Wiley & Sons, 2012).
[12]G. Dresselhaus, A. F. Kip, and C. Kittel, "Cyclotron resonance of electrons and holes in silicon and germanium crystals," Phys. Rev. **98**, 368 (1955).
[13]N. Kamaraju, W. Pan, U. Ekenberg, D. M. Gvozdić, S. Boubanga-Tombet, P. C. Upadhya, J. Reno, A. J. Taylor, and R. P. Prasankumar, "Terahertz magneto-optical spectroscopy of a two dimensional hole gas," Appl. Phys. Lett. **106**, 031902 (2015).
[14]M. Failla, J. Keller, G. Scalari, C. Maissen, J. Faist, C. Reichl, W. Wegscheider, O. J. Newell, D. R. Leadley, M. Myronov, and J. Lloyd-Hughes, "Terahertz quantum Hall effect for spin-split heavy-hole gases in strained Ge quantum wells," New J. Phys. **18**, 113036 (2016).
[15]J. E. Dill, C. F. C. Chang, D. Jena, and H. G. Xing, "Two-carrier model-fitting of Hall effect in semiconductors with dual-band occupation: A case study in GaN two-dimensional hole gas," J. Appl. Phys. **137**, 025702 (2025).
[16]J. Simon, V. Protasenko, C. Lian, H. Xing, and D. Jena, "Polarization-induced hole doping in wide–band-gap uniaxial semiconductor heterostructures," Science **327**, 60–64 (2010).
[17]S. J. Bader, R. Chaudhuri, M. F. Schubert, H. W. Then, H. G. Xing, and D. Jena, "Wurtzite phonons and the mobility of a GaN/AlN 2D hole gas," Appl. Phys. Lett. **114**, 253501 (2019).
[18]A. Legros, K. W. Post, P. Chauhan, D. G. Rickel, X. He, X. Xu, X. Shi, I. Bozovic, S. A. Crooker, and N. P. Armitage, "Evolution of the cyclotron mass with doping in $La_{2-x}Sr_xCuO4$," Phys. Rev. B **106**, 195110 (2022).
[19]K. W. Post, A. Legros, D. G. Rickel, J. Singleton, R. D. McDonald, X. He, I. Bozovic, X. Xu, X. Shi, N. P. Armitage, and S. A. Crooker, "Observation of

cyclotron resonance and measurement of the hole mass in optimally-doped $La_{2-x}Sr_xCuO4$," Phys. Rev. B **103**, 134515 (2021).
[20]R. J. B. Dietz, N. Vieweg, T. Puppe, A. Zach, B. Globisch, T. Göbel, P. Leisching, and M. Schell, "All fiber-coupled THz-TDS system with kHz measurement rate based on electronically controlled optical sampling," Opt. Lett. **39**, 6482 (2014).
[21]G. T. Noe, Q. Zhang, J. Lee, E. Kato, G. L. Woods, H. Nojiri, and J. Kono, "Rapid scanning terahertz time-domain magnetospectroscopy with a table-top repetitive pulsed magnet," Appl. Opt. **53**, 5850 (2014).
[22]B. Cheng, P. Taylor, P. Folkes, C. Rong, and N. P. Armitage, "Magnetoterahertz response and faraday rotation from massive Dirac fermions in the topological crystalline insulator $Pb_{0.5}Sn_{0.5}Te$," Phys. Rev. Lett. **122**, 097401 (2019).
[23]E. D. Palik and J. K. Furdyna, "Infrared and microwave magnetoplasma effects in semiconductors," Rep. Prog. Phys. **33**, 1193 (1970).
[24]M. C. Nuss and J. Orenstein, in *Millimeter and Submillimeter Wave Spectroscopy of Solids*, edited by G. Grüner (Springer-Verlag, 1998), pp. 7–50.
[25]M. V. Kartsovnik, "High magnetic fields: A tool for studying electronic properties of layered organic metals," Chem. Rev. **104**, 5737 (2004).
[26]N. Harrison and J. Singleton, "On the de Haas-van Alphen effect in inhomogeneous alloys," J. Phys.: Condens. Matter **13**, L463 (2001).
[27]J. Singleton, *Band Theory and Electronic Properties of Solids* (Oxford University Press, Oxford, 2001).
[28]L. Krückeberg, S. Wirth, V. Solovyev, A. Grosser, I. V. Kukushkin, T. Mikolajick, and S. Schmult, "Quantum and transport lifetimes in optically induced GaN/AlGaN 2DEGs grown on bulk GaN," J. Vac. Sci. Technol., B **38**, 042203 (2020).
[29]D. Pines and P. Nozieres, *The Theory of Quantum Liquids* (Benjamin, New York, 1966).
[30]W. Kohn, "Cyclotron resonance and de Haas-van Alphen oscillations of an interacting electron gas," Phys. Rev. **123**, 1242 (1961).
[31]K. Kanki and K. Yamada, "Theory of cyclotron resonance in interacting electron systems on the basis of the fermi liquid theory," J. Phys. Soc. Jpn. **66**, 1103 (1997).
[32]A. H. MacDonald and C. Kallin, "Cyclotron resonance in two dimensions: Electron-electron interactions and band nonparabolicity," Phys. Rev. B **40**, 5795 (1989).